

## Nonlinear studies on the effect of non-uniform heat generation/absorption on hydromagnetic flow of nanofluid over a vertical plate

Abdul Kafoor Abdul Hakeem<sup>a</sup>, Bhose Ganga<sup>b</sup>, Sait Mohamed Yusuff Ansari<sup>c</sup>,  
Nagaraj Vishnu Ganesh<sup>a</sup>, Mohammad Mansur Rahman<sup>d</sup>

<sup>a</sup>Department of Mathematics, Sri Ramakrishna Mission Vidyalaya College of Arts & Science, Coimbatore - 641 020, India

<sup>b</sup>Department of Mathematics, Providence College for Women, Coonoor - 643 104, India

<sup>c</sup>Department of Mathematics, Jamal Mohamed College, Trichy - 6420 020, India

<sup>d</sup>Department of Mathematics and Statistics, College of Science, Sultan Qaboos University, PO Box 36, PC 123 Al-Khod, Muscat, Sultanate of Oman  
mansurdu@yahoo.com

**Received:** March 6, 2015 / **Revised:** November 30, 2015 / **Published online:** December 2, 2016

**Abstract.** The analytical and numerical studies are performed to investigate the non-uniform heat generation/absorption effect on the boundary layer flow of an incompressible, electrically conducting nanofluid over a vertical plate in the presence of thermal radiation. The highly nonlinear governing equations along with the boundary conditions are converted into ordinary differential equations by appropriate similarity transformations. The transformed highly nonlinear ordinary differential equations are solved both analytically and numerically using homotopy analysis method and fourth-order Runge–Kutta method with shooting technique, respectively, for the various values of physical parameters. The results show that the presence of both space and temperature dependent heat generation enhances the velocity and temperature profiles and reduces the solid volume fraction of nanofluid profile. Comparison between present analytical and numerical results is found to be good.

**Keywords:** homotopy analysis method, hydromagnetic flow, nanofluid, non-uniform heat generation/absorption, thermal radiation, vertical plate.

### 1 Introduction

Nonlinear phenomena play a crucial role in applied mathematics and physics. It is difficult to solve nonlinear problems, especially to obtain the analytical solutions. An analytical method for strongly nonlinear problems, namely the homotopy analysis method (HAM) was proposed by Liao in 1992 [11]. HAM is a general analytic approach to get series

solutions of various types of nonlinear equations, including algebraic equations, ordinary differential equations, partial differential equations, differential-integral equations, differential-difference equations and coupled equations of them. Unlike perturbation method, the HAM is independent of small or large physical parameters and thus is valid no matter whether a nonlinear problem contains small or large physical parameters or not. More importantly, different from all perturbation and traditional non-perturbation methods, the HAM provides us a simple way to ensure the convergence of solution series, and therefore, the HAM is valid even for strongly nonlinear problems. Besides, the HAM provides us with great freedom to choose proper base functions to approximate a nonlinear problem [11, 12, 14].

The study of flow and internal heat generation/absorption has many practical applications in manufacturing processes in industry. In thermal convection process, the effect of heat generation/absorption is important where there exists high temperature difference between the surface and the ambient fluid. The deposition rate in nuclear reactors, electronic chips and semi conductor wafers is altered by heat generation. In many theoretical studies on heat transfer and fluid flow problems, the internal heat generation/absorption is assumed to be constant, space-dependent or temperature-dependent (non-uniform heat source/sink). The following researchers studied the effect of space and temperature dependent internal heat generation/absorption on the fluid flow problems recently [6, 7, 15, 19].

Nanofluids are suspensions of nanoparticles (usually 1–100 nm) in fluids, which were introduced by Choi [5] that show significant enhancement of their properties at modest nanoparticles concentration. Many of the publications on nanofluids are about understanding their behavior so that they can be utilized where straight heat transfer enhancement is paramount as in many industrial applications such as nuclear reactors, transportation, electronics as well as biomedicine and food. Boungiorno et al. [3] proposed an analytical model for convective transport in nanofluids taking into the account of Brownian diffusion and thermophoresis. The following papers investigated the nanofluid flow problems over a vertical plate with various physical effects numerically using Boungiorno model in the absence of space and temperature dependent heat generation/absorption [1, 4, 8–10, 16–18, 20, 21, 23, 24].

Keeping this in mind, we have performed both analytical and numerical investigation on the problem of heat transfer of hydromagnetic nanofluid flow over vertical plate in the presence of thermal radiation, space and temperature dependent internal heat generation/absorption. The nonlinear governing equations along with the boundary conditions are converted into ordinary differential equations by appropriate similarity transformations. The transformed equations are solved both analytically and numerically using homotopy analysis method and fourth-order Runge–Kutta method with shooting technique, respectively.

## 2 Formulation of the problem

We consider steady two-dimensional boundary layer flow of a nanofluid over vertical plate in the presence of magnetic field intensity, thermal radiation and volumetric rate of

heat generation/absorption. We select a coordinate frame, in which the  $x$ -axis is aligned vertically upwards. We consider a vertical plate at  $y = 0$ . At this boundary, the temperature  $T$  and the nanoparticles volume fraction  $\phi$  take constant values  $T_w$  and  $\phi_w$ , respectively. When  $y \rightarrow \infty$ , the temperature  $T$  and the nanoparticles volume fraction of the nanofluid  $\phi$  take values  $T_\infty$  and  $\phi_\infty$ , respectively. We consider the influence of a constant magnetic field of strength  $B_0$  that is applied along the normal direction of the plate. It is further assumed that the induced magnetic field strength is negligible in comparison to the applied magnetic field. Under the above assumptions, the boundary layer equations governing the flow, thermal and concentration fields can be written in dimensional form as [10]

$$\frac{\partial u}{\partial x} + \frac{\partial v}{\partial y} = 0, \tag{1}$$

$$\begin{aligned} \frac{\partial p}{\partial x} = & \mu \frac{\partial^2 u}{\partial y^2} - \rho_f \left( u \frac{\partial u}{\partial x} + v \frac{\partial u}{\partial y} \right) - \sigma B_0^2 u \\ & + [(1 - \phi_\infty)\rho_{f\infty}\beta g(T - T_\infty) - (\rho_p - \rho_{f\infty})g(\phi - \phi_\infty)], \end{aligned} \tag{2}$$

$$\begin{aligned} u \frac{\partial T}{\partial x} + v \frac{\partial T}{\partial y} = & \alpha \nabla^2 T - \frac{1}{(\rho c)_f} \frac{\partial q_r}{\partial y} + \frac{1}{(\rho c)_f} q''' \\ & + \tau \left[ D_B \frac{\partial \phi}{\partial y} \frac{\partial T}{\partial y} + \frac{D_T}{T_\infty} \left( \frac{\partial T}{\partial y} \right)^2 \right], \end{aligned} \tag{3}$$

$$u \frac{\partial \phi}{\partial x} + v \frac{\partial \phi}{\partial y} = D_B \frac{\partial^2 \phi}{\partial y^2} + \frac{D_T}{T_\infty} \frac{\partial^2 T}{\partial y^2}, \tag{4}$$

where  $u$  and  $v$  are the velocity components along the  $x$  and  $y$  directions, respectively.  $p$  is the fluid pressure,  $\rho_f$  is the density of base fluid,  $\rho_p$  is the nanoparticle density,  $\mu$  is the absolute viscosity of the base fluid,  $\alpha = k/(\rho c)_f$  is the thermal diffusivity of the base fluid,  $\tau = (\rho c)_p/(\rho c)_f$  is the ratio of nanoparticles heat capacity and the base fluid heat capacity,  $\phi$  is the local solid volume fraction of the nanofluid,  $\beta$  is volumetric thermal expansion coefficient of the base fluid,  $D_B$  is the Brownian diffusion coefficient,  $D_T$  is the thermophoretic diffusion coefficient,  $T$  is the local temperature and  $g$  is the acceleration due to gravity.  $B_0$  is the constant magnetic field, and  $q'''$  is the space and temperature dependent internal heat generation/absorption (non-uniform heat source/sink), which can be expressed as [6, 7, 15, 19]

$$q''' = \frac{kRa_x^{1/2}}{2x^2} [A(T_w - T_\infty)s'(\eta) + B(T - T_\infty)],$$

where  $A$  and  $B$  are the parameters of the space and temperature dependent internal heat generation/absorption,  $s$  is defined in Eq. (8). It is to be noted that  $A$  and  $B$  are positive to internal heat source and negative to internal heat sink. The boundary conditions are taken to be

$$\begin{aligned} u = 0, \quad v = 0, \quad T = T_w, \quad \phi = \phi_w \quad \text{at } y = 0, \\ u = v = 0, \quad T \rightarrow T_\infty, \quad \phi \rightarrow \phi_\infty \quad \text{as } y \rightarrow \infty. \end{aligned}$$

The radiative heat flux  $q_r$  is described by Roseland approximation [5, 6] such that

$$q_r = -\frac{4\sigma^*}{3\delta} \frac{\partial T^4}{\partial y}, \quad (5)$$

where  $\sigma^*$  and  $\delta$  are the Stefan–Boltzmann constant and the mean absorption coefficient, respectively. We assume that the temperature differences within the flow are sufficiently small so that the  $T^4$  can be expressed as a linear function after using Taylor series to expand  $T^4$  about the free stream temperature  $T_\infty$  and neglecting higher-order terms. This result is the following approximation:

$$T^4 \cong 4T_\infty^3 T - 3T_\infty^4. \quad (6)$$

Using (5) and (6) in (3), we obtain

$$\begin{aligned} u \frac{\partial T}{\partial x} + v \frac{\partial T}{\partial y} = & \alpha \nabla^2 T + \frac{1}{(\rho c)_f} \frac{16\sigma^* T_\infty^3}{3\delta} \frac{\partial^2 T}{\partial y^2} + \frac{1}{(\rho c)_f} q''' \\ & + \tau \left[ D_B \frac{\partial \phi}{\partial y} \frac{\partial T}{\partial y} + \frac{D_T}{T_\infty} \left( \frac{\partial T}{\partial y} \right)^2 \right]. \end{aligned} \quad (7)$$

### 3 Similarity transformations

The following similarity transformations are introduced to transform Eqs. (2), (4) and (7) into ordinary differential equations:

$$\begin{aligned} \eta = \frac{y}{x} \text{Ra}_x^{1/4}, \quad \psi = \alpha \text{Ra}_x^{1/4} s(\eta), \\ \theta(\eta) = \frac{T - T_\infty}{T_w - T_\infty}, \quad f(\eta) = \frac{\phi - \phi_\infty}{\phi_w - \phi_\infty} \end{aligned} \quad (8)$$

with the local Rayleigh number, which is defined as

$$\text{Ra}_x = \frac{(1 - \phi_\infty)g\beta(T_w - T_\infty)x^3}{\nu\alpha},$$

and the stream function  $\psi(x, y)$  is defined such that

$$u = \frac{\partial \psi}{\partial y}, \quad v = -\frac{\partial \psi}{\partial x}.$$

So, the continuity equation (1) is identically satisfied. After some algebraic manipulation, the momentum, energy and the solid volume fraction equations are obtained as follows:

$$s''' + \frac{1}{4\text{Pr}} (3ss'' - 2s'^2 - 4M\sqrt{\text{Pr}}s') + \theta - \text{Nrf} = 0, \quad (9)$$

$$\left(1 + \frac{4N}{3}\right)\theta'' + \frac{3}{4}s\theta' + \text{Nb}f'\theta' + \text{Nt}\theta'^2 + \frac{1}{2}[As' + B\theta] = 0, \quad (10)$$

$$f'' + \frac{3}{4}\text{Les}f' + \frac{\text{Nt}}{\text{Nb}}\theta'' = 0, \quad (11)$$

where primes denote differentiation with respect to  $\eta$ , and the non-dimensional parameters, Prandtl number  $Pr$ , buoyancy-ratio parameter  $Nr$ , Brownian motion parameter  $Nb$ , thermophoresis parameter  $Nt$ , Lewis number  $Le$ , radiation parameter  $N$ , heat generation or absorption parameters  $A$  and  $B$  and magnetic field parameter  $M$  are defined as follows:

$$Pr = \frac{\nu}{\alpha}, \quad Nr = \frac{(\rho_p - \rho_{f\infty})(\phi_w - \phi_\infty)}{\rho_{f\infty}\beta(T_w - T_\infty)(1 - \phi_\infty)},$$

$$Nb = \frac{(\rho c)_p D_B (\phi_w - \phi_\infty)}{(\rho c)_f \alpha}, \quad Nt = \frac{(\rho c)_p D_T (T_w - T_\infty)}{(\rho c)_f \alpha T_\infty},$$

$$Le = \frac{\alpha}{D_B}, \quad M = \frac{\sigma B_0^2 x^{1/2}}{\rho_f \sqrt{(1 - \phi_\infty)g\beta(T_w - T_\infty)}}, \quad N = \frac{4\sigma^* T_\infty^3}{k\delta}.$$

It is to be mentioned that due to the  $x$ -dependence of the magnetic field parameter  $M$ , Eq. (9) is locally similar. A choice of  $B_0 \sim x^{-1/4}$  eliminates the dependence of  $M$  on  $x$ , thus, Eq. (9) becomes self similar.

The corresponding boundary conditions are as follows:

$$s(\eta) = 0, \quad s'(\eta) = 0, \quad \theta(\eta) = 1, \quad f(\eta) = 1 \quad \text{at } \eta = 0, \quad (12)$$

$$s'(\eta) = 0, \quad \theta(\eta) = 0, \quad f(\eta) = 0 \quad \text{as } \eta \rightarrow \infty. \quad (13)$$

A quantities of practical interest are the Nusselt number  $Nu$  and Sherwood number  $Sh$  defined by

$$Nu = \frac{xq_w''}{k(T_w - T_\infty)}, \quad Sh = \frac{xq_m''}{D_B(\phi_w - \phi_\infty)},$$

where  $q_w''$  and  $q_m''$  are the wall heat flux and mass flux. Following Kuznetsov and Nield [10], the reduced local Nusselt number  $Nu_r$  and reduced local Sherwood number  $Sh_r$  can be introduced and represented as follows:

$$Nu_r = Ra_x^{1/4} Nu = -\left(1 + \frac{4N}{3}\right)\theta'(0), \quad Sh_r = Ra_x^{1/4} Sh = -f'(0).$$

#### 4 Analytical solution by homotopy analysis method

Equations (9)–(11) are solved under the corresponding boundary conditions (12) and (13) by using HAM. For HAM solutions, we choose the initial guesses and auxiliary linear operators in the following form:

$$s_0(\eta) = 1 - e^{-\eta} - \eta e^{-\eta}, \quad \theta_0(\eta) = e^{-\eta}, \quad f_0(\eta) = e^{-\eta},$$

$$L_1(s) = s''' - s', \quad L_2(\theta) = \theta'' + \theta, \quad L_3(f) = f'' + f,$$

$$L_1(c_1 + c_2 e^\eta + c_3 e^{-\eta}) = L_2(c_1 e^\eta + c_2 e^{-\eta}) = L_3(c_1 e^\eta + c_2 e^{-\eta}) = 0,$$

where  $c_1$ ,  $c_2$  and  $c_3$  are constants. Let  $p \in [0, 1]$  be the embedding parameter, and  $h_1$ ,  $h_2$  and  $h_3$  are the non-zero auxiliary parameters. We then construct the following problems: zeroth-order deformation problems

$$\begin{aligned}(1-p)L_1[s(\eta, p) - s_0(\eta)] &= ph_1N_1[s(\eta, p), \theta(\eta, p), f(\eta, p)], \\ (1-p)L_2[\theta(\eta, p) - \theta_0(\eta)] &= ph_2N_2[s(\eta, p), \theta(\eta, p), f(\eta, p)], \\ (1-p)L_3[f(\eta, p) - f_0(\eta)] &= ph_3N_3[s(\eta, p), \theta(\eta, p), f(\eta, p)], \\ s(0, p) = 0, \quad s'(\infty, p) &= 1, \quad s'(\infty, p) = 0, \\ \theta(0, p) = 1, \quad \theta(\infty, p) &= 0, \\ f(0, p) = 1, \quad f(\infty, p) &= 0\end{aligned}$$

and

$$\begin{aligned}N_1[s(\eta, p), \theta(\eta, p), f(\eta, p)] &= s'''(\eta, p) + \frac{1}{4Pr}(3s(\eta, p)s''(\eta, p) - 2s'^2(\eta, p) \\ &\quad - 4M\sqrt{Pr}s'(\eta, p)) + \theta(\eta, p) - Nrf(\eta, p), \\ N_2[s(\eta, p), \theta(\eta, p), f(\eta, p)] &= \left(1 + \frac{4N}{3}\right)\theta''(\eta, p) + \frac{3}{4}s(\eta, p)\theta'(\eta, p) \\ &\quad + Nb f'(\eta, p)\theta'(\eta, p) + Nt\theta'^2(\eta, p) \\ &\quad + \frac{1}{2}[As'(\eta, p) + B\theta(\eta, p)], \\ N_3[s(\eta, p), \theta(\eta, p), f(\eta, p)] &= f''(\eta, p) + \frac{3}{4}Les(\eta, p)f'(\eta, p) + \frac{Nt}{Nb}\theta''(\eta, p).\end{aligned}$$

For  $p = 0$  and  $p = 1$ , we have

$$\begin{aligned}s(\eta, 0) &= s_0(\eta), & s(\eta, 1) &= s(\eta), \\ \theta(\eta, 0) &= \theta_0(\eta), & \theta(\eta, 1) &= \theta(\eta), \\ f(\eta, 0) &= f_0(\eta), & f(\eta, 1) &= f(\eta).\end{aligned}$$

Due to Taylor's series with respect to  $p$ , we have

$$\begin{aligned}s(\eta, p) &= s_0(\eta) + \sum_{m=1}^{\infty} s_m(\eta)p^m, \\ \theta(\eta, p) &= \theta_0(\eta) + \sum_{m=1}^{\infty} \theta_m(\eta)p^m, \\ f(\eta, p) &= f_0(\eta) + \sum_{m=1}^{\infty} f_m(\eta)p^m,\end{aligned}$$

$$s_m(\eta) = \frac{1}{m!} \frac{\partial^m (s(\eta, p))}{\partial p^m},$$

$$\theta_m(\eta) = \frac{1}{m!} \frac{\partial^m (\theta(\eta, p))}{\partial p^m},$$

$$f_m(\eta) = \frac{1}{m!} \frac{\partial^m (f(\eta, p))}{\partial p^m},$$

and thus,  $m$ th-order deformation problems

$$L_1 [s_m(\eta) - \chi_m s_{m-1}(\eta)] = h_1 R_m^s(\eta),$$

$$L_2 [\theta_m(\eta) - \chi_m \theta_{m-1}(\eta)] = h_2 R_m^\theta(\eta),$$

$$L_3 [f_m(\eta) - \chi_m f_{m-1}(\eta)] = h_3 R_m^f(\eta)$$

and

$$s_m(0) = s'_m(0) = s'_m(\infty) = 0,$$

$$\theta_m(0) = \theta_m(\infty) = 0,$$

$$f_m(0) = f'_m(\infty) = 0,$$

where

$$R_m^s = s'''_{m-1} + \frac{1}{4Pr} \left( 3 \sum_{i=0}^{m-1} s_{m-1-i} s''_i - 2 \sum_{i=0}^{m-1} s'_{m-1-i} s'_i - 4M\sqrt{Pr} s'_{m-1} \right) + \theta_{m-1} - Nr f_{m-1},$$

$$R_m^\theta = \left( 1 + \frac{4N}{3} \right) \theta''_{m-1} + \frac{3}{4} \sum_{i=0}^{m-1} s_{m-1-i} \theta'_i + Nb \sum_{i=0}^{m-1} f'_{m-1-i} \theta'_i + Nt \sum_{i=0}^{m-1} \theta'_{m-1-i} \theta'_i + \frac{1}{2} [As'_{m-1} + B\theta_{m-1}],$$

$$R_m^f = f''_{m-1} + \frac{3}{4} Le \sum_{i=0}^{m-1} s_{m-1-i} f'_i + \frac{Nt}{Nb} \theta''_{m-1}.$$

Here  $\chi_m = 0$  for  $m \leq 1$  and  $\chi_m = 1$  for  $m > 1$ ;  $h$  is chosen in such a way that these three series are convergent at  $p = 1$ . Therefore, we have

$$s(\eta) = s_0(\eta) + \sum_{m=1}^{\infty} s_m(\eta),$$

$$\theta(\eta) = \theta_0(\eta) + \sum_{m=1}^{\infty} \theta_m(\eta),$$

$$f(\eta) = f_0(\eta) + \sum_{m=1}^{\infty} f_m(\eta).$$

#### 4.1 Convergence of HAM

As pointed by Liao [14], the convergence rate of approximation for the HAM solution strongly depends on the values of auxiliary parameter. It is essential to adopt a proper value of the auxiliary parameters  $h_1$ ,  $h_2$  and  $h_3$ , which can adjust and control the convergence of the HAM solution. The range of the  $h$  curves of the functions  $s''(0)$ ,  $\theta'(0)$  and  $f'(0)$  for 15th order of approximations is shown in Fig. 1. It is found that the range of the admissible values of  $h_1$ ,  $h_2$  and  $h_3$  are  $-1.6 \leq h_1 \leq 0.1$ ,  $-1.4 \leq h_2 \leq 0.0$ ,  $-1.4 \leq h_3 \leq 0.0$ .

$$\text{Res}_s = s''' + \frac{1}{4\text{Pr}}(3ss'' - 2s'^2 - 4M\sqrt{\text{Pr}}s') + \theta - \text{Nr}f, \quad (14)$$

$$\text{Res}_\theta = \left(1 + \frac{4N}{3}\right)\theta'' + \frac{3}{4}s\theta' + \text{Nb}f'\theta' + \text{Nt}\theta'^2 + \frac{1}{2}[As' + B\theta], \quad (15)$$

$$\text{Res}_f = f'' + \frac{3}{4}\text{Les}f' + \frac{\text{Nt}}{\text{Nb}}\theta''. \quad (16)$$

In order to choose the optimal value of auxiliary parameter  $h$ , we have presented the average residual error as (see [13, 22] for more details)

$$\Delta_{s,m} = \frac{1}{K} \sum_{i=0}^K \left[ \text{Res}_s \left( \sum_{j=0}^m s_j(i\Delta x) \right) \right]^2,$$

$$\Delta_{\theta,m} = \frac{1}{K} \sum_{i=0}^K \left[ \text{Res}_\theta \left( \sum_{j=0}^m \theta_j(i\Delta x) \right) \right]^2,$$

$$\Delta_{f,m} = \frac{1}{K} \sum_{i=0}^K \left[ \text{Res}_f \left( \sum_{j=0}^m f_j(i\Delta x) \right) \right]^2,$$

where  $\Delta x = 10/K$  and  $K = 15$ . For the given order of approximation  $m$ , the optimal value of  $h$  is given by the minimum values of  $\Delta_{s,m}$ ,  $\Delta_{\theta,m}$  and  $\Delta_{f,m}$  corresponding to the

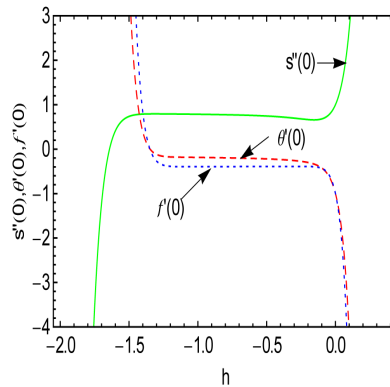


**Figure 1.**  $s''(0)$ ,  $\theta'(0)$  and  $f'(0)$  plots for determining of optimum of  $h$  coefficient at 15th order of approximation.

nonlinear algebraic equations:

$$\frac{d\Delta_{s,m}}{dh} = 0, \quad \frac{d\Delta_{\theta,m}}{dh} = 0, \quad \frac{d\Delta_{f,m}}{dh} = 0.$$

In the present calculation,  $h = h_1 = h_2 = h_3 = -0.35$  for the whole region  $\eta$ .

## 5 Numerical method for solution

The nonlinear coupled differential equations (9)–(11) along with the boundary conditions (12)–(13) form a two point boundary value problem and is solved using shooting technique together with fourth-order Runge–Kutta integration scheme by converting it into an initial value problem. In this method, we have to choose a suitable finite value of  $\eta \rightarrow \infty$ , say  $\eta_\infty$ . Considering  $y_1 = s$ ,  $y_4 = \theta$ , and  $y_6 = f$ , we set the following first-order system:

$$\begin{aligned} y_1' &= y_2, & y_2' &= y_3, \\ y_3' &= -\frac{1}{4\text{Pr}}(3y_1y_3 - 2y_2^2 - 4M\sqrt{\text{Pr}}y_2) - y_4 + N_r y_6, & y_4' &= y_5, \\ y_5' &= \left(-\frac{3}{4}y_1y_5 - \text{Nb}y_7y_5 - \text{Nt}y_5^2 - \frac{1}{2}(Ay_2 + By_4)\right) \frac{3}{3 + 4N}, & (17) \\ y_6' &= y_7, & y_7' &= -\frac{3}{4}\text{Le}y_1y_7 - \frac{\text{Nt}}{\text{Nb}}y_5' \end{aligned}$$

with the boundary conditions

$$y_1(0) = 0, \quad y_2(0) = 0, \quad y_4(0) = 1 \quad \text{and} \quad y_6(0) = 1. \quad (18)$$

To solve (17) with (18) as an initial value problem, we must need the values for  $y_3(0)$  i.e.  $s''(0)$ ,  $y_5(0)$  i.e.  $\theta'(0)$  and  $y_7(0)$  i.e.  $f'(0)$ , but no such values are given. The initial guess values for  $s''(0)$ ,  $\theta'(0)$  and  $f'(0)$  are chosen and the fourth-order Runge–Kutta integration scheme is applied to obtain the solution. Then we compare the calculated values of  $s'(\eta)$ ,  $\theta(\eta)$  and  $f(\eta)$  at  $\eta_\infty$  with the given boundary conditions  $s'(\eta_\infty) = 0$ ,  $\theta(\eta_\infty) = 0$  and  $f(\eta_\infty) = 0$  and adjust the values of  $s''(0)$ ,  $\theta'(0)$  and  $f'(0)$  using the shooting technique to give better approximation for the solution. The process is repeated until we get the results correct up to the desired accuracy of  $10^{-8}$  level, which fulfills the convergence criterion.

## 6 Results and discussion

Equations (9)–(11) subject to the boundary conditions (12)–(13) are solved both analytically and numerically. The results are discussed through graphical illustrations for some values of the governing parameters  $\text{Pr}$ ,  $\text{Le}$ ,  $M$ ,  $A$ ,  $B$ ,  $N$ ,  $N_r$ ,  $\text{Nb}$  and  $\text{Nt}$ . In order to verify the accuracy of our present study, the values of the reduced Nusselt number  $\text{Nu}_r = \text{Ra}_x^{1/4}\text{Nu}$  in the limiting case of a regular fluid for various values of Prandtl

**Table 1.** Test results.

Pr	$Nu_r = Ra_x^{1/4} Nu$		
	Bejan [2]	Present results: analytical, numerical	
1	0.401	0.40103	0.40102817
10	0.465	0.46496	0.46496287
100	0.490	0.49000	0.49000028

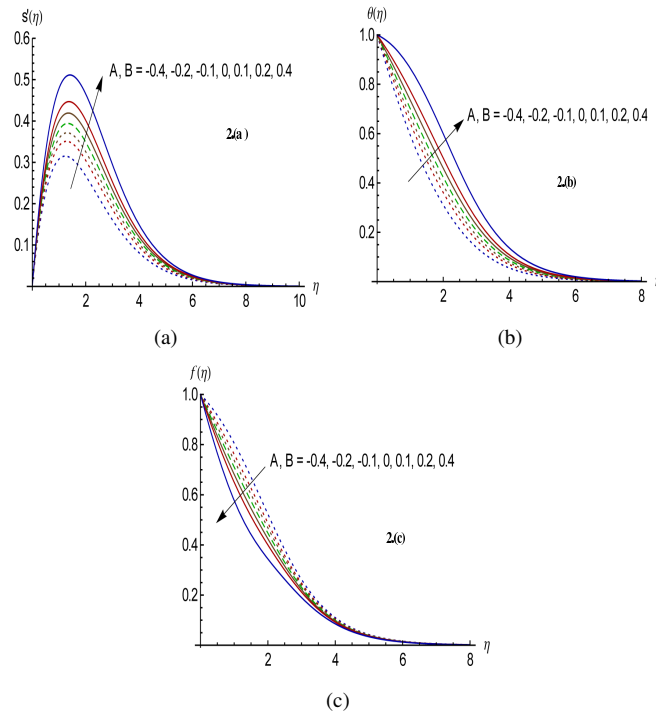


**Figure 2.** Effect of heat generation/absorption parameter on (a) dimensionless velocity profile (b) dimensionless temperature profile (c) dimensionless solid volume fraction of the nanofluid profile with  $Pr = 1$ ,  $Le = 1$ ,  $M = N = 0.5$  and  $Nb = Nt = Nr = 0.1$ .

number are compared and displayed in Table 1, which shows an excellent agreement with those reported by Bejan [2].

Figure 2 demonstrates the effect of space and temperature dependent heat generation/absorption parameters on the velocity, temperature and solid volume fraction of nanofluid profiles, respectively. It is observed that the increasing values of both heat generation parameters ( $A > 0$  and  $B > 0$ ) lead to increase the velocity (Fig. 2a) and temperature profiles (Fig. 2b) and decreases the solid volume fraction of nanofluid profile (Fig. 2c). A reverse trend has been observed for increasing values of heat absorption parameters ( $A < 0$  and  $B < 0$ ). Due to the fact that the presence of space and temperature dependent heat generation enhances the momentum and thermal boundary layers thicknesses and reduces the nanofluid concentration boundary layer thickness.

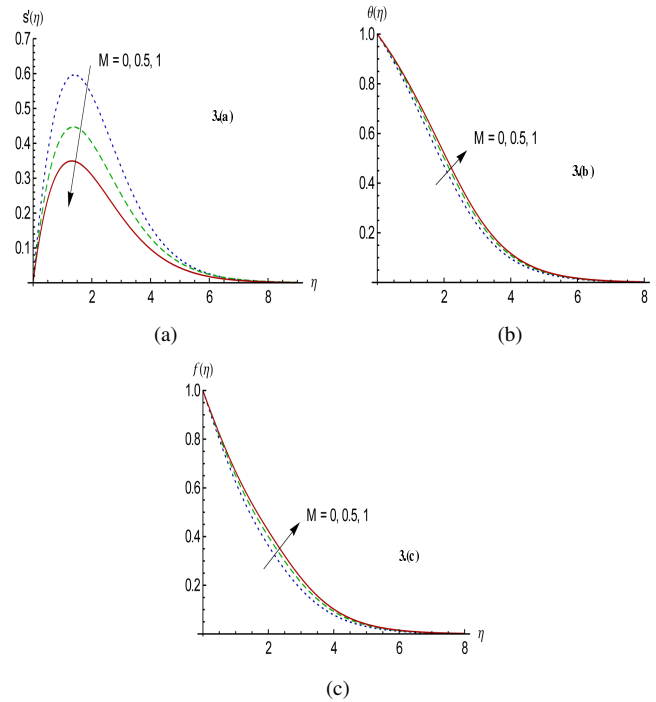


**Figure 3.** Effect of magnetic parameter on (a) dimensionless velocity profile (b) dimensionless temperature profile (c) dimensionless solid volume fraction of the nanofluid profile with  $Pr = 1, Le = 1, N = 0.5, A = B = 0.2$  and  $Nb = Nt = Nr = 0.1$ .

The effect of magnetic parameter on the velocity, temperature and solid volume fraction profiles of nanofluid is illustrated in Fig. 3. The velocity profile diminishes with the increase of magnetic parameter (Fig. 3a). The temperature and solid volume fraction profiles (Figs. 3b and 3c) increase in the presence of magnetic parameter. This is because a drag-like Lorentz force is created by the transverse magnetic field on the electrically conducting fluid. This force has the tendency to slow down the flow and increase the temperature and solid volume fraction profiles of the nanofluid.

Figure 4 shows the effect of thermal radiation parameter on the velocity, temperature and solid fraction of nanofluid profiles. It is observed that the increasing values of radiation parameter increase the velocity and temperature profiles (Figs. 4a and 4b) and reduce the solid volume fraction of nanofluid profile (Fig. 4c).

The effect of Brownian motion and thermophoresis parameters on the velocity, temperature and solid volume fraction of nanofluid profiles is depicted in Fig. 5. It is noticed that the velocity and temperature profiles (Fig. 5a and 5b) increase with the increase of  $Nb$  and  $Nt$ . Due to the fact that the thermophoresis parameter  $Nt$  is directly proportional to the heat transfer coefficient associated with the nanofluid. It is observed from Fig. 5c, the solid volume fraction of nanofluid profile decreases with the increase of Brownian motion and thermophoresis parameters.

The values of the reduced Nusselt number and the local Sherwood number for different values of physical parameters are tabulated in Table 2. The reduced Nusselt number and the local Sherwood number increase with the increasing values of  $Pr$ ,  $Le$  and decrease with  $M$  and  $Nr$ . The increasing values of  $N$ ,  $Nb$  and  $Nt$  decrease the reduced Nusselt number and increase the local Sherwood number. The space and temperature dependent heat generation parameter decreases the reduced Nusselt number and increases the local Sherwood number. An opposite trend is observed in heat absorption case.

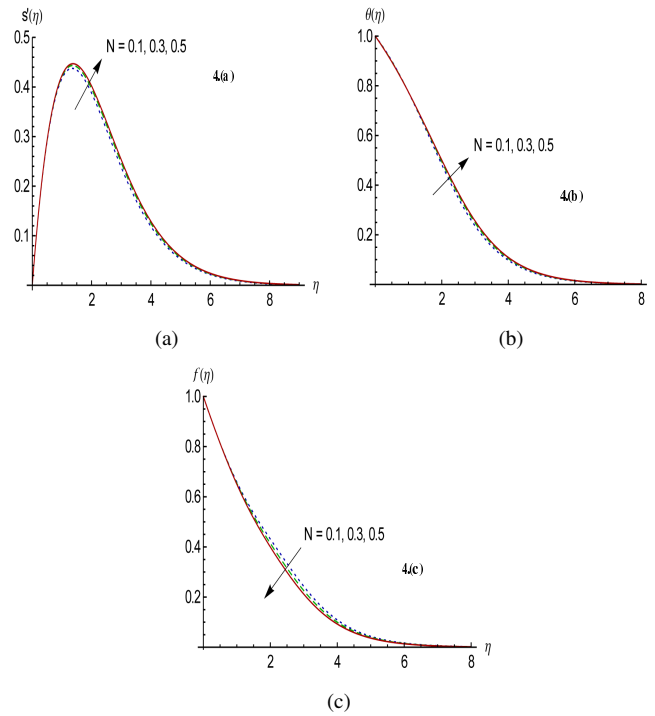


**Figure 4.** Effects of radiation parameter on (a) dimensionless velocity profile (b) dimensionless temperature profile (c) dimensionless solid volume fraction of the nanofluid profile with  $Pr = 1$ ,  $Le = 1$ ,  $M = 0.5$ ,  $\lambda = 0.1$  and  $Nb = Nt = Nr = 0.1$ .

**Table 2.** Values of  $Nu_r$  and  $Sh_r$ . While studying the effect of individual parameters, the following values are assumed:  $M = 0.4$ ,  $N = 0.2$ ,  $Pr = 2$ ,  $Le = 3$ ,  $A = B = 0.2$ ,  $Nr = 0.3$  and  $Nb = Nt = 0.6$ .

Parameters	Values	$Nu_r$		$Sh_r$	
		Analytical	Numerical	Analytical	Numerical
$M$	0.2	0.09711	0.09710535	0.78412	0.78411889
	0.4	0.08642	0.08642488	0.76128	0.76128103
	0.6	0.07641	0.07640703	0.74131	0.74131095
$N$	0.1	0.07724	0.07724455	0.76833	0.76832625
	0.2	0.08642	0.08642488	0.76128	0.76128103
	0.3	0.09356	0.09355816	0.75590	0.75589610

Table 2. (Continued.)

Parameters	Values	Nu <sub>r</sub>		Sh <sub>r</sub>	
		Analytical	Numerical	Analytical	Numerical
Pr	1	0.06558	0.06557969	0.72460	0.72460278
	2	0.08642	0.08642488	0.76128	0.76128103
	3	0.09581	0.09581089	0.78213	0.78212636
Le	1	0.08571	0.08570693	0.47458	0.47458155
	3	0.08642	0.08642488	0.76128	0.76128103
	5	0.08722	0.08721566	0.91955	0.91954889
A	-0.2	0.17561	0.17561218	0.67251	0.67251068
	0	0.13559	0.13559884	0.71501	0.71501128
	0.2	0.08642	0.08642488	0.76128	0.76128103
B	-0.2	0.24424	0.24424189	0.61238	0.61238097
	0	0.16928	0.16927741	0.68554	0.68553680
	0.2	0.08642	0.08642488	0.76128	0.76128103
Nr	0.1	0.09256	0.09255960	0.77869	0.77868667
	0.2	0.08955	0.08954690	0.77012	0.77012485
	0.3	0.08642	0.08642488	0.76128	0.76128103
Nb = Nt	0.3	0.13108	0.13107506	0.72201	0.72201342
	0.6	0.08643	0.08642488	0.76128	0.76128103
	0.9	0.05179	0.05178774	0.79027	0.79027452

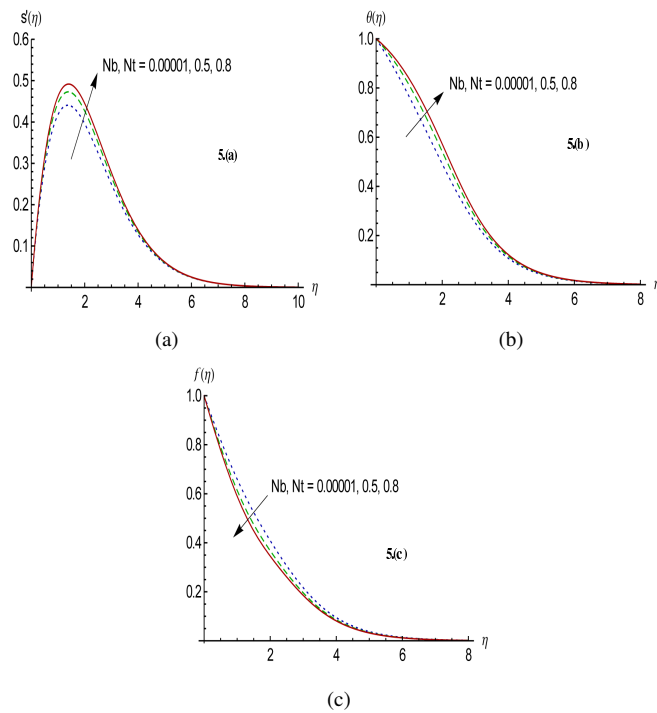


Figure 5. Effects of Brownian motion and thermophoresis parameters on (a) dimensionless velocity profile (b) dimensionless temperature profile (c) dimensionless solid volume fraction of the nanofluid profile with Pr = 1, Le = 1, Nr = 0.1, A = B = 0.2 and M = N = 0.5.

## 7 Conclusions

A two-dimensional steady free convective hydromagnetic laminar incompressible boundary layer flow of an electrically conducting nanofluid past a vertical plate with the effects of thermal radiation in the presence of non-uniform heat source or sink is studied both analytically and numerically. Homotopy analysis method is used to find the analytical solutions, whereas numerical solutions are obtained by fourth-order Runge–Kutta method with shooting technique for the governing nonlinear dimensionless ordinary differential equations. The main conclusions derived from the present study are as follow:

- The increasing values of radiation, Brownian motion and thermophoresis parameters enhance the nanofluid velocity and temperature profiles and diminish the solid volume fraction profile.
- The presence of magnetic field reduces the velocity and solid volume fraction profiles and enhances the temperature profile.
- The velocity and temperature profiles increase in the presence of space and temperature dependent heat generation and decreases in heat absorption case. The solid volume fraction profile increases in the presence of heat absorption and decreases in heat generation case.
- The space and temperature dependent heat absorption parameters increase the reduced Nusselt number and decrease the local Sherwood number, but both space and temperature dependent heat generation parameters show an opposite effect on the reduced Nusselt number and the local Sherwood number.
- The space and temperature dependent heat absorption case is better suited for cooling purposes.

## References

1. A.A. Afify, M.A.A. Bazid, Effects of variable fluid properties on the natural convective boundary layer flow of a nanofluid past a vertical plate: Numerical study, *J. Comput. Theor. Nanosci.*, **11**(1):210–218, 2014.
2. A. Bejan, *Convection Heat Transfer*, Wiley, New York, 1984.
3. J. Buongiorno, Convective transport in nanofluids, *J. Heat Transfer*, **128**(3):240–250, 2006.
4. A.J. Chamka, A.M. Rashad, C.R. Reddy, P.V.S.N. Murthy, Effect of suction/injection on free convection along a vertical plate in a nanofluid saturated non-Darcy porous medium with internal heat generation, *Indian J. Pure Appl. Math.*, **45**(3):321–342, 2014.
5. S.U.S. Choi, J.A. Eastman, Enhancing thermal conductivity of fluids with nanoparticles, in D.A. Siginer, H.P. Wang (Eds.), *Developments and Applications of Non-Newtonian Flows. 1995 International Mechanical Engineering Congress and Exhibition, San Francisco, CA, November 12–17, 1995*, ASME, 1995, pp. 99–105.
6. A.K. Abdul Hakeem, N. Vishnu Ganesh, B. Ganga, Effect of heat radiation in a Walter's liquid B fluid over a stretching sheet with non-uniform heat source/sink and elastic deformation, *J. King Saud Univ. - Eng. Sci.*, **26**(2):168–175, 2014.

7. A.K. Abdul Hakeem, R. Kalaivanan, N. Vishnu Ganesh, B. Ganga, Effect of partial slip on hydromagnetic flow over a porous stretching sheet with non-uniform heat source/sink, thermal radiation and wall mass transfer, *Ain Shams Eng. J.*, **5**(3):913–922, 2014.
8. W.A. Khan, A. Aziz, Natural convection flow of a nanofluid over a vertical plate with uniform surface heat flux, *Int. J. Therm. Sci.*, **50**(7):1207–1214, 2011.
9. M. Kumari, R.S.R. Gorla, Effect of melting on mixed convective boundary layer flow over a vertical plate embedded in a porous medium saturated with a nanofluid, *J. Nanofluids*, **4**(1):82–90, 2015.
10. A.V. Kuznetsov, D.A. Nield, Natural convective boundary layer flow of a nanofluid past a vertical plate, *Int. J. Therm. Sci.*, **49**(2):243–247, 2010.
11. S. Liao, *Beyond Perturbation: Introduction to the Homotopy Analysis Method*, Chapman & Hall/CRC Press, Boca Raton, FL, 2000.
12. S.J. Liao, On the homotopy analysis method for nonlinear problems, *Appl. Math. Comput.*, **147**(2):499–513, 2004.
13. S.J. Liao, An optimal homotopy-analysis approach for strongly nonlinear differential equations, *Commun. Nonlinear Sci. Numer. Simul.*, **15**(8):2003–2016, 2010.
14. S.J. Liao, Y. Tan, A general approach to obtain series solutions of nonlinear differential equations, *Stud. Appl. Math.*, **119**(4):297–355, 2007.
15. M.M. Nandeppanavar, M.S. Abel, J. Tawade, Heat transfer in a Walter's liquid B fluid over an impermeable stretching sheet with non-uniform heat source/sink and elastic deformation, *Commun. Nonlinear Sci. Numer. Simul.*, **15**(7):1791–1802, 2010.
16. A. Noghrehabadi, M. Ghalambaz, A. Ghanbarzadeh, Effects of variable viscosity and thermal conductivity on natural-convection of nanofluids past a vertical plate in porous media, *J. Mech.*, **30**(3):265–275, 2014.
17. M.M. Rahman, I.A. Eltayeb, Radiative heat transfer in a hydromagnetic nanofluid past a non-linear stretching surface with convective boundary condition, *Meccanica*, **48**(3):601–615, 2013.
18. M.M. Rahman, T. Grosan, I. Pop, Oblique stagnation-point flow of a nanofluid past a shrinking sheet, *Int. J. Numer. Methods Heat Fluid Flow*, **26**:1–27, 2016.
19. M.M. Rahman, I. Pop, Unsteady boundary layer flow and heat transfer over a permeable shrinking sheet with non-uniform heat source, in *Proceedings of the 19th Australasian Fluid Mechanics Conference, Melbourne, Australia, December 8–11, 2014*, Paper No. 533.
20. M.M. Rahman, A.V. Rosca, I. Pop, Boundary layer flow of a nanofluid past a permeable exponentially shrinking/stretching surface with second order slip using Buongiorno's model, *Int. J. Heat Mass Transfer*, **77**:1133–1143, 2014.
21. M.M. Rahman, A.V. Rosca, I. Pop, Boundary layer flow of a nanofluid past a permeable exponentially shrinking surface with convective boundary condition using buongiorno's model, *Int. J. Numer. Methods Heat Fluid Flow*, **5**:299–319, 2015.
22. M.M. Rashidi, B. Rostami, N. Freidoonimehr, S. Abbasbandey, Free convective heat and mass transfer for MHD fluid flow over a permeable vertical stretching sheet in the presence of the radiation and buoyancy effects, *Ain Shams Eng. J.*, **5**(3):901–912, 2014.

23. M.A. Sheremet, M.M. Rahman I. Pop, Three-dimensional natural convection in a porous enclosure filled with a nanofluid using Buongiorno's mathematical model, *Int. J. Heat Mass Transfer*, **8**:396–405, 2015.
24. D. Srinivasacharya, O. Surender, Effect of double stratification on mixed convection boundary layer flow of a nanofluid past a vertical plate in a porous medium, *Appl. Nanosci.*, **5**(1):29–38, 2014.